Sci

MDPI

Article

Differentiation of Heterogeneous Mouse Liver from HCC by Hyperpolarized ^{13}C Magnetic Resonance

Naama Lev-Cohain †, Gal Sapir †, Sivaranjan Uppala, Atara Nardi-Schreiber, Shraga Nahum Goldberg, Yael Adler-Levy, Jacob Sosna, J. Moshe Gomori and Rachel Katz-Brull *

Department of Radiology, Hadassah Medical Center, The Faculty of Medicine, Hebrew University of Jerusalem, Kalman Mann 1, Jerusalem 9112001, Israel

* Correspondence: rkb@hadassah.org.il; Tel.: +972-26-776-582

† These authors contributed equally to this work.

Abstract: The clinical characterization of small hepatocellular carcinoma (HCC) lesions in the liver and differentiation from heterogeneous inflammatory or fibrotic background is important for early detection and treatment. Metabolic monitoring of hyperpolarized ^{13}C-labeled substrates has been suggested as a new avenue for diagnostic magnetic resonance. The metabolism of hyperpolarized [1-^{13}C]pyruvate was monitored in mouse precision-cut liver slices (PCLS) of aged MDR2-KO mice, which served as a model for heterogeneous liver and HCC that develops similarly to the human disease. The relative in-cell activities of lactate dehydrogenase (LDH) to alanine transaminase (ALT) were found to be 0.40 ± 0.06 (n = 3) in healthy livers (from healthy mice), 0.90 ± 0.27 (n = 3) in heterogeneously inflamed liver, and 1.84 ± 0.46 (n = 3) in HCC. Thus, the in-cell LDH/ALT activities ratio was found to correlate with the progression of the disease. The results suggest that the LDH/ALT activities ratio may be useful in the assessment of liver disease. Because the technology used here is translational to both small liver samples that may be obtained from image-guided biopsy (i.e., ex vivo investigation) and to the intact liver (i.e., in a noninvasive MRI scan), these results may provide a path for differentiating heterogeneous liver from HCC in human subjects.

Keywords: lactate dehydrogenase; alanine transaminase; MDR2 knockout; dissolution dynamic nuclear polarization; perfused precision cut liver slices

Citation: Lev-Cohain, N.; Sapir, G.; Uppala, S.; Nardi-Schreiber, A.; Goldberg, S.N.; Adler-Levy, Y.; Sosna, J.; Gomori, J.M.; Katz-Brull, R. Differentiation of Heterogeneous Mouse Liver from HCC by Hyperpolarized ^{13}C Magnetic Resonance. *Sci* **2021**, *3*, 8. https://doi.org/10.3390/sci3010008

Received: 13 December 2019
Accepted: 24 December 2020
Published: 8 January 2021

1. Introduction

Hepatocellular carcinoma (HCC) is the most common primary liver cancer [1], and cirrhosis increases the risk of developing this malignancy. With the development of HCC from regenerative and dysplastic nodules (present in the cirrhotic liver) to tumor nodules [2], there is a need to characterize focal findings and to evaluate their potential aggressiveness. Hence, the role of diagnostic imaging is growing continuously.

Hyperpolarized ^{13}C magnetic resonance imaging (MRI), i.e., MRI that is based on hyperpolarized substrate metabolism, can be made to target the aberrant metabolism of cancer. Such MRI monitoring of hyperpolarized substrate metabolism relies, by-and-large, on the dissolution-dynamic nuclear polarization technique (dDNP) [3] with hyperpolarized ^{13}C-labeled pyruvate analogs as the most widely used substrates and the only agents approved for human use [4–10].

Lactate dehydrogenase (LDH) is commonly found to be elevated in cancerous tissues [11] as malignant cells have up-regulation of LDH A (LDHA) [12]. This is potentially relevant for tissue characterization and for monitoring tumor growth and treatment response in the liver. Another important liver enzyme is alanine transaminase (ALT). This enzyme is present in almost all cells, with high expression in liver cells [13]. ALT is considered one of the most liver-specific enzymes amongst serological markers [14], as its serum level is among the most important tests for evaluation of liver injury [15,16]. Both

LDH and ALT activities can be monitored by following the metabolism of hyperpolarized [1-^{13}C]pyruvate in liver tissues [17–27]. While LDH activity may be correlated to malignant processes, ALT activity may reflect the healthy liver physiology. We hypothesized that evaluation of the ratio of LDH and ALT activities in healthy and diseased liver tissues may provide a useful parameter for liver disease characterization and could potentially differentiate malignant from background heterogeneous inflamed and fibrotic liver.

To test this hypothesis, we investigated the hyperpolarized [1-^{13}C]pyruvate metabolism in the liver of healthy mice (Institute for Cancer Research (ICR); Caesarean Derived-1(CD1)) and of aged MDR2-knockout mice (MDR2-KO). MDR2-KO is a well-established model of chronic inflammatory liver disease in which heterogeneous liver inflammation and fibrosis, and HCC tumors, develop spontaneously [28–30]. Mouse liver tissues were investigated here ex vivo, in the form of precision cut liver slices (PCLS) [31,32], using a recently developed methodology for studying hyperpolarized substrate metabolism in these isolated liver tissues in well-perfused conditions [21]. In addition, we used a unique acquisition approach that is based on hyperpolarized product selective saturating excitations [33] to determine the absolute value of the enzyme activities ratio in real-time, in the living cells.

2. Results

Hyperpolarized [1-^{13}C]pyruvate metabolism was studied in PCLS of the following three groups: Group 1, healthy livers; Group 2, heterogeneously inflamed liver; and Group 3, HCC. Photographs that show the typical appearance of these livers are shown in Figure 1.

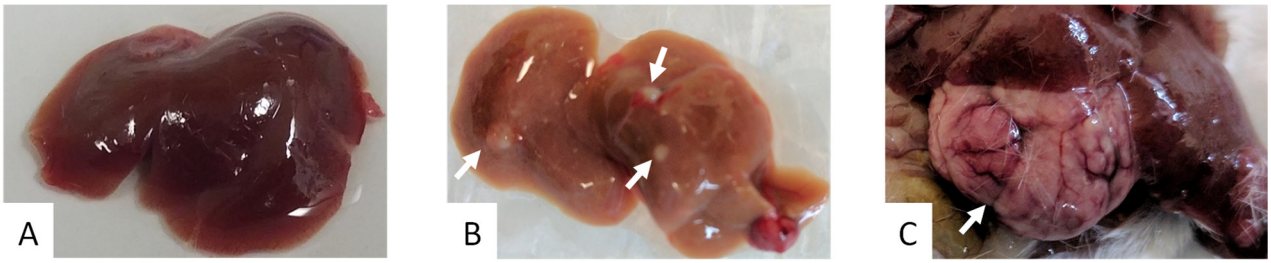

Figure 1. Typical appearance of the three groups of liver tissues under investigation. (**A**) A healthy mouse liver. (**B**) A heterogeneously inflamed liver with small nodules ca. 0.5–1 mm in size (arrows) and a cirrhotic gross appearance. (**C**) A HCC tumor (arrow) in the liver. (**B**,**C**) were obtained from aged MDR2-KO mice.

The formation of [1-^{13}C]lactate and [1-^{13}C]alanine following an injection of hyperpolarized [1-^{13}C]pyruvate was demonstrated on ^{13}C NMR spectra recorded from the perfused PCLS in all groups in real-time. Typical examples of the spectra, enzymatic rates, and histological appearance are shown in Figure 2. Enzyme activity was determined as the production rate of [1-^{13}C]lactate and [1-^{13}C]alanine following an injection of [1-^{13}C]pyruvate (Materials and Methods). Typical results are shown in Figure 2. In the ^{13}C spectrum of PCLS taken from the liver of a healthy mouse, the [1-^{13}C]lactate signal is smaller than that of the [1-^{13}C]alanine (Figure 2A). For this spectrum, the ratio of LDH/ALT enzymatic activities was 0.26 (Figure 2D). The histological appearance of the normal liver is characterized by normal hepatocytes with a small heterochromatic nucleus (Figure 2G, blue arrows) and hepatic sinusoids (Figure 2G, green arrows). A spectrum recorded from PCLS of an aged MDR2-KO mouse heterogeneous liver with no dominant lesion is shown in Figure 2B. In this spectrum, the ratio of the [1-^{13}C]lactate signal to the [1-^{13}C]alanine signal is higher compared to the spectrum of PCLS taken from a healthy liver. The calculated LDH/ALT activity ratio for this spectrum was 0.79 (Figure 2E), and the histological appearance is less organized compared with the normal liver, with less heterochromatic nuclei (Figure 2H, blue arrows). A typical ^{13}C spectrum from PCLS of a HCC tumor from the liver of an aged MDR2-KO mouse is shown in Figure 2C. The [1-^{13}C]lactate signal was higher than that of [1-^{13}C]alanine, and the LDH/ALT activity ratio was 2.42 (Figure 2F). The histological appearance is characterized by disrupted tissue architecture manifested as a larger nucleus-

to-cytoplasm ratio compared to the other groups and large euchromatic nuclei (Figure 2I, red arrows).

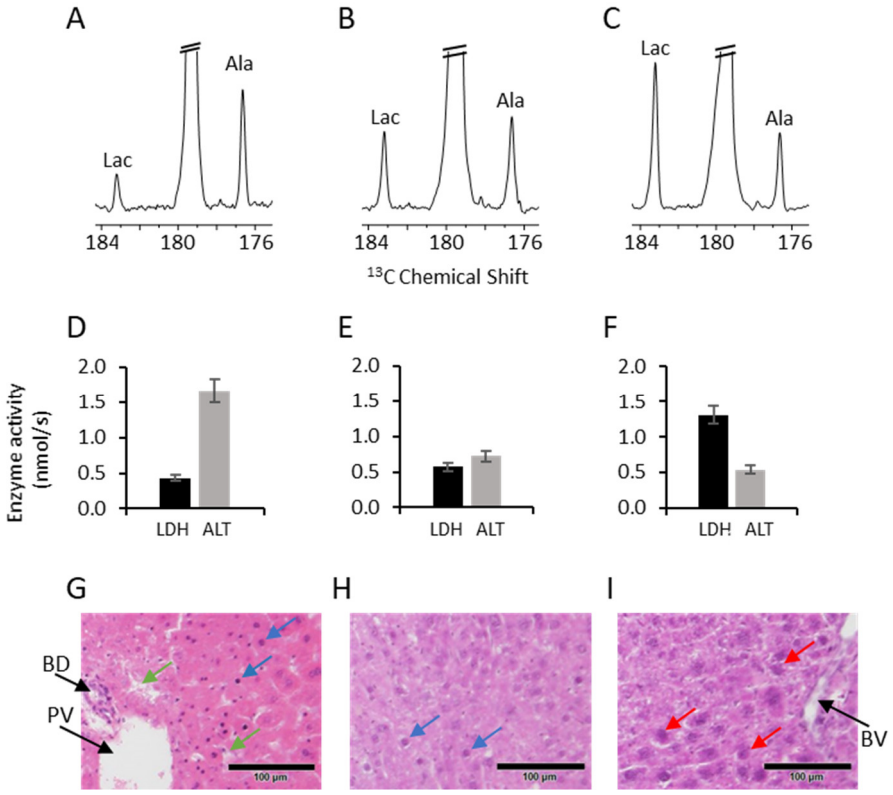

Figure 2. Typical ^{13}C spectra, enzyme activities, and histological preparations of precision-cut liver slices (PCLS) from a healthy mouse, and MRD2-KO mice with heterogeneous liver and HCC tumors. Panels (**A**–**C**) show ^{13}C spectra acquired at specific times following the injection of [1-^{13}C]pyruvate to PCLS obtained from a normal mouse (**A**, at 41 s), an aged MDR2 KO mouse with heterogeneous liver (**B**, at 32 s), and an aged MDR2-KO mouse with a HCC tumor in the liver (**C**, at 32 s). The spectra were processed with 5 Hz exponential multiplication, zero filled from 16,384 to 65,536 points, and baseline corrected. Ala, [1-^{13}C]alanine; Lac, [1–13]lactate. The [1-^{13}C]pyruvate hydrate signal at 179.35 is truncated. Panels (**D**–**F**) show the enzymatic activity of lactate dehydrogenase (LDH) and alanine transaminase (ALT) calculated from the spectra shown in (**A**–**C**), respectively. The error bars show a 10% error which was estimated based on the signal-to-noise ratio in the spectra. Panels (**G**–**I**) demonstrates typical histological preparations from the PCLS that were perfused in the spectrometer and used for the metabolic study. The tissues were taken for histology many hours after harvesting—at the end of the study, which consisted of several hours of perfusion in the spectrometer. For this reason, the quality of the preparation for light microscopy is reduced. (**G**) Liver of a healthy mouse, with hepatic sinusoids (green arrows), and normal hepatocytes with small heterochromatic nuclei (blue arrows). (**H**) Heterogeneous liver of an aged MDR2-KO mouse, with hepatocytes with less heterochromatic nuclei (blue arrows). (**I**) A HCC tumor from the liver of an aged MDR2-KO mouse, with hepatocytes with large euchromatic nuclei (red arrows). Bar size is 100 µm; PV, portal vein; BD, bile duct; BV, blood vessel.

Altogether, we performed a total of 19 injections to PCLS taken from 9 mice (3 from each group). For each injection, the LDH/ALT activity ratio was calculated as an average of all the time points selected for this analysis as described in the Materials and Methods section. Then, for each sample (from a single mouse), this ratio was averaged over all injections performed (1 to 3). A summary of the entire data set is provided in Table 1 in the Materials and Methods section. The LDH/ALT activities ratio was found to be lowest for the PCLS taken from livers of healthy mice (0.40 ± 0.06, $n = 3$), intermediate for PCLS

taken from heterogeneous livers of aged MDR2-KO mice (0.90 ± 0.27, n = 3), and highest for the tissue taken from the HCC tumors in the livers of aged MDR2-KO mice (1.84 ± 0.46, n = 3). The LDH/ALT activities ratio of each group was found to be significantly different from the other two groups (Figure 3).

Table 1. Parameters used for enzymatic rate calculations per animal per injection of hyperpolarized [1-^{13}C]pyruvate.

Mouse Number	Group	Injection Number	Number of Spectral Recordings Used for Rate Calculation	ρ [1-^{13}C]Alanine	ρ [1-^{13}C]Lactate
1	Healthy Liver	1 [a]	1	0.559	0.559
		1 [a,c]	2	0.276	0.276
2		2 [a]	2	0.292	0.292
		3 [a]	2	0.292	0.292
3		2 [a]	1 [d]	0.375	0.375
		3 [a]	1 [e]	0.375	0.375
4	Heterogeneous Liver	1 [b]	5	0.062	0.058
		2 [b]	6	0.062	0.058
		3 [b]	2	0.062	0.058
5		1 [b,c]	4	0.062	0.058
		2 [b]	3	0.062	0.058
6		1 [b]	2	0.062	0.058
		2 [b]	2	0.062	0.058
7	HCC	1 [b]	6	0.244 [f]	0.217 [f]
		2 [b]	8	0.244 [f]	0.217 [f]
8		1 [b]	5	0.062	0.058
		2 [b,c]	4	0.062	0.058
9		1 [b]	1	0.062	0.058
		2 [b]	1	0.062	0.058

[a] Acquired with a 3 ms Gaussian pulse. [b] Acquired with a 2.5 ms Sinc pulse. [c] Included in Figure 2. [d] The maximum signal intensity from the sum of two spectra was used in this calculation due to low signal-to-noise ratio (SNR). [e] The integrated intensity from the sum of two spectra was used in this calculation due to low SNR. [f] The ρ values were different due to a different pulse offset that was used.

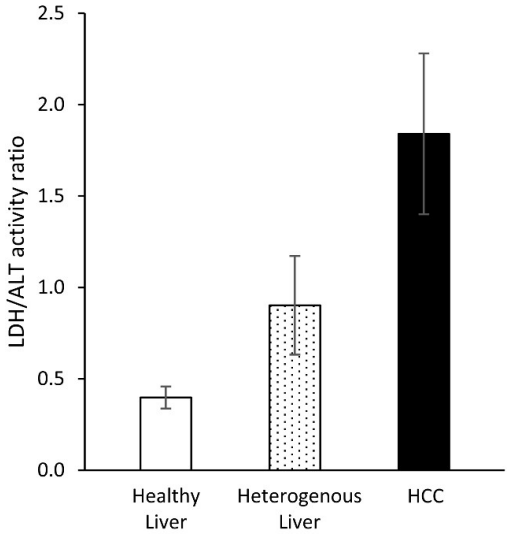

Figure 3. The LDH to ALT activities ratio in PCLS from normal liver, heterogeneous liver, and HCC tumors in the liver. Normal livers were obtained from healthy mice (white bar). Heterogeneous livers (dotted bar) and HCC tumors of the liver (black bars) were obtained from aged MDR2-KO mice which typically show progressive liver disease [29]. The enzymatic activity was calculated following an injection of hyperpolarized [1-^{13}C]pyruvate. LDH and ALT activities were determined by the production rate of hyperpolarized [1-^{13}C]lactate and [1-^{13}C]alanine, respectively. The error bars mark the standard deviation between animals within each group (n = 3 for all groups). The significance of the differences between the groups was assessed with one tailed t-tests with the following results: Healthy livers vs. Heterogeneous livers, p = 0.031; Heterogeneous livers vs. HCC tumors, p = 0.033, Healthy livers vs. HCC tumors, p = 0.006.

3. Discussion

Our results suggest that the ratio of the in-cell activities of LDH and ALT may potentially assist in identifying HCC tumors within the heterogeneous liver. This refers specifically to the case of heterogeneity that results from chronic inflammation and fibrosis, as these conditions are modeled in the liver of aged MDR2-KO mice. This animal model was selected for the current study because it represents human disease progression and allows evaluation and monitoring of increased fibrosis in the surrounding inflamed liver and its progression into HCC. The MDR2-KO mice lack the liver-specific glycoprotein, P-glycoprotein, which is responsible for phosphatidylcholine transport across the bile canalicular membrane [29]. Its absence causes portal inflammation, which starts at an early age and continues to fibrosis, leading to multiple nodules which fulfill the microscopic criteria used in chemically induced hepatocarcinogenesis to diagnose neoplastic nodules [29]. The liver inflammation and toxicity lead to the development of hepatocyte dysplasia—a premalignant condition—by the age of 12 months, which progresses with time to the formation of multiple scattered tumors in most of the mice by the age of 16 months [28,29]. MDR2-KO mice aged 12 months and older were chosen for the current study, to increase the likelihood of obtaining diseased liver tissue with the presence of heterogeneity and tumors. Indeed, both large tumors (>2 cm) and heterogeneity (visible 0.5–1 mm nodules and discoloration) were found in the livers of these aged MDR2-KO mice during surgery. This visual categorization during surgery was based on the assumption that the larger the lesion, the higher the likelihood of pathological development [34], which was later confirmed by histology. The two-group approach within the aged mice was intended to assist in translation of the results to potential studies of the human liver.

Although we sampled metabolism over a tissue volume of about 0.5 cc, which may appear large in terms of ^{1}H-MRI spatial resolution, we note that this sampling volume is relevant to clinical hyperpolarized MRI, considering a nominal voxel size as low as 7 × 7 × 10 mm reported in previous studies [7,34]. Thus, the summation over the liver tissue in both the heterogeneous liver and the HCC tumors groups is likely to represent the potential clinical setting.

The LDH/ALT activities ratio determined here is, in principle, a parameter that is translational to in vivo studies and clinical studies, provided that the product-selective saturating excitation acquisition approach [21,33] can be implemented in vivo. The ability to detect only newly synthesized hyperpolarized metabolites in each repetition time enables this enzyme activity quantification. Moreover, the use of enzyme activities ratio nulls the need for assumptions regarding the number of viable tissues and partial volume effects across studies, as both in-cell enzymatic activities (LDH and ALT) originate from the same tissue.

Both LDH and ALT are known to increase in the blood during hepatocellular damage, and both are highly expressed in the liver [13,35]. LDH is commonly found to be elevated in cancerous tissues and is incorporated in prognostic scores of several solid tumors and therapies [11,34,36–38]. ALT is among the most liver-specific enzymes [14], and its level is among the most important serological markers for liver injury evaluation and prognosis [15,16,39]. Therefore, the trend found here for the LDH/ALT activity ratio, where an increase in this value is correlated to the progression of the malignant disease, appears to be well in agreement with previous findings and characterization of these enzymes in liver diseases. It appears highly likely that this activities ratio could turn out to be useful for differentiation of heterogeneous liver from HCC.

Liver metabolism was studied using hyperpolarized substrates in various pre-clinical models [18–24]. Previous pre-clinical studies on HCC using hyperpolarized metabolites include two studies on orthotopically implanted McA-RH7777 cells in rats. Darpolor et al. [5] suggested increased [1-^{13}C]pyruvate metabolism to [1-^{13}C]lactate and [1-^{13}C]alanine in the HCC tumors compared to the normal liver tissue, and Duwel et al. [4] showed the synthesis of [1-^{13}C]lactate and [1-^{13}C]alanine before and after transcatheter arterial embolization (TAE) of the tumor. Recently, a specific study on liver fibrosis was carried out

by Chung-Man et al. [35] who measured the metabolic signals of [1-^{13}C]lactate and [1-^{13}C]alanine in cirrhotic livers and found increased ratios of [1-^{13}C]lactate/[1-^{13}C]pyruvate and [1-^{13}C]alanine/[1-^{13}C]pyruvate in mild and severe fibrotic liver. In all of the studies cited above, the absolute LDH/ALT enzyme activities ratio was not determined. Such an absolute determination of enzyme activities ratio was made possible recently with the product-selective saturation excitation approach [21,33] which was applied here. Therefore, due to the complexity of interpreting enzyme activities ratios from hyperpolarized metabolite signals, these prior results cannot be directly compared to the current results except for the presence of these enzyme activities in HCC and liver tissues. This is due to the fact that previously only the signal ratio was reported, whereas here the actual enzyme activities ratio was quantified. The latter provides a robust measure that is independent of kinetic modeling and differences in intracellular longitudinal relaxation time (T_1) of the metabolic species. In addition, the differences between the pre-clinical models also prohibits direct comparison to prior results: here, we used the MDR2-KO model, where the malignancy that develops closely resembles the human disease associated with better survival [28]. However, the model of orthotopic transplantation of McA-RH7777 cells utilizes aggressive HCC cells [4,5]. This leads to two main biological differences: a) the tumor aggressiveness is lower in the current study and b) the current study consists of liver parenchyma that is heterogeneous (in Group 2) and uninvolved (in Group 1) as opposed to only uninvolved parenchyma in the McA-RH7777 model.

We note two limitations in our study: (1) The relatively small sample size in each group may limit the strength of the results. In this regard, we note that despite the small sample size, there are significant differences between the three groups. In practice, MDR2-KO mice do not survive well beyond 9–11 months, and this limits the number of animals one can obtain at these ages (per Group). (2) The diseased mice were sampled as two categories only. It is possible that sampling within further time frames during the disease progression may provide additional knowledge about the relationship between the LDH/ALT enzyme activity ratio and disease progression.

In conclusion, we have shown a potential role for the LDH/ALT enzyme activity ratio in assessment of liver disease. These results may be promising for better characterization of the heterogeneous liver and HCC diagnosis, using hyperpolarized MR, especially in the setting of cirrhosis or inflammatory liver disease.

4. Conclusions

Determination of relative in-cell enzymatic activities in mouse liver ex vivo enabled differentiation between HCC, heterogeneous liver tissue, and healthy liver. This is a unique translational capability of hyperpolarized substrate metabolic monitoring offered by dDNP-MR.

5. Materials and Methods

5.1. Materials

The OX063 radical (GE Healthcare, UK) was obtained from Oxford Instruments Molecular Biotools (Oxford, UK). [1-^{13}C]pyruvic acid was purchased from Sigma-Aldrich, (Rehovot, Israel) and from Cambridge Isotope Laboratories (Tewksbury, MA, USA). Choline chloride, histidine, NaCl, and KCl were purchased from Sigma-Aldrich, (Rehovot, Israel). Isoflurane was obtained from the Hebrew University Authority for Biological and Biomedical Models. Waymouth medium: Waymouth MB 752/1 medium in powder form (Sigma-Aldrich, Rehovot, Israel) was supplemented with 1.79 mM choline chloride and 0.82 mM histidine and dissolved to the final volume recommended by the supplier as previously described [21].

5.2. Animals, Surgery, Tissue Processing and Categorization

The joint ethics committee (IACUC) of the Hebrew University and Hadassah Medical Center approved the study protocol for animal welfare (Protocol Number MD-17-15048-5).

The Hebrew University is an AAALAC International accredited institute. Three male (Institute for Cancer Research (ICR); Caesarean Derived-1 (CD1)) mice weighing 35 ± 4 g, 3–4 months of age, were used for evaluation of normal liver tissue. Six male MDR2-KO mice over the age of 12 months, weighing 41 ± 1 g, were used for evaluation of diseased livers. Anesthesia was performed with isoflurane using a gas anesthesia system (Somnosuite, Kent Scientific, Torrington, CT, USA). After general anesthesia was achieved, the peritoneum and the liver were exposed via a midline laparotomy. The anatomic landmarks such as the main vessels-portal vein, inferior vena cava, and hepatic artery were identified, and then the liver was separated and quickly excised and placed in ice-cold Waymouth medium.

For the healthy mice, the excised liver was cut into about 10 pieces which were placed in the ice-cold Waymouth medium for holding. Each piece was sliced to PCLS as described below. These samples comprised the PCLS category termed here Group 1, healthy livers. For the MDR2-KO mice, the liver was visually examined and evaluated for its nodularity, contour, and exophytic mass during surgery and categorized according to the liver appearance. We used two categories: (1) livers with diffuse visible tissue heterogeneity and no dominant mass, and (2) livers that presented with a dominant exophytic large tumor (over the size of 2 cm). A typical appearance of these two groups is shown in Figure 1. For the former category (termed here Group 2, heterogeneous liver), the tissue was characterized by a nodular appearance, with the presence of multiple ca. 0.5–1 mm size nodules. A representing segment of the liver was cut, and the PCLS were prepared as described below. For the latter category (termed here Group 3, HCC), only the mass was harvested. The mass was then cut and sliced to PCLS as described below. All cut tissues were placed in ice-cold Waymouth medium for holding until the PCLS preparation was completed. The residual liver tissue was placed in formalin.

5.3. PCLS Preparation

PCLS were prepared as described previously [21]. Each liver segment was sliced using a McIlwain tissue chopper (Mickle, UK) to 500 µm slices and placed in ice-cold Waymouth medium.

5.4. PCLS Perfusion in the Spectrometer

The PCLS in ice-cold Waymouth medium were transferred to a 10 mm NMR tube and perfused therein continuously at a rate of 4 mL/min with Waymouth medium at 35–36 °C. The sample was placed in an NMR spectrometer (5.8 T, RS2D, Mundolsheim, France) under continuous perfusion. The temperature of the medium inside the NMR tube was monitored with an NMR compatible temperature probe (Osensa, BC, Canada).

5.5. Hyperpolarization and Dissolution

Spin polarization and fast dissolution were carried out in a dDNP polarizer (HyperSense, Oxford Instruments Molecular Biotools, Oxford, UK) operating at 3.35 T. Microwave frequency of 94.110–94.120 GHz was applied for the polarization of a [1-^{13}C]pyruvic acid formulation at 1.40 to 1.49 K. The formulations consisted of 14.0 mM OX063 radical in the neat acid. The amount of [1-^{13}C]pyruvic acid formulation placed in the polarization cup was 5 ± 0.5 mg. The dissolution medium consisted of 4 mL of 50 mM phosphate buffer which contained 19 mM TRIS and 138.6 mM NaCl. The pH of the dissolution medium was adjusted with NaOH such that upon mixing with the pyruvic acid in the cup the final pH was 7.4.

5.6. Histological Study of the Same PCLS Batch Used for the Metabolic Study

Following the metabolic study, the PCLS were freeze clamped in liquid nitrogen. The samples were stored at −20 °C until further processing. Prior to histological sectioning, the slices were defrosted and placed in formalin for 1 day. Sectioning and Hematoxylin and Eosin staining was performed by the Pathology staff.

5.7. Determination of Enzyme Activities

The activities of the LDH and ALT enzymes were determined as the production rate of hyperpolarized [1-^{13}C]lactate and [1-^{13}C]alanine, respectively, using the product-selective saturation excitation approach [21,33]. The rate of product formation, ν_{prod}, in nmol/s units was calculated using Equation (1) from the integrated intensity, S_{prod}, relative to that of [1-^{13}C]pyruvate, S_{pyr}, taking into account (1) the ratio of product and [1-^{13}C]pyruvate relative response to the selective excitation pulse (response coefficient, ρ, Table 1); (2) the repetition time (TR, in s units); (3) the concentration of hyperpolarized [1-^{13}C]pyruvate in the extracellular medium in mM units, $[Pyr]$, ca. 14 mM; and (4) the volume of the extracellular hyperpolarized medium within the probe in mL units (V, estimated at 0.5 mL).

$$\nu_{prod} = \frac{S_{prod}}{S_{pyr\_product}} \cdot \frac{\rho}{\mathrm{TR}} \cdot [Pyr] \cdot V \cdot 1000 \quad (1)$$

The rate of each product formed, ν_{lac} and ν_{ala}, respectively, was calculated from each product's integrated signal intensity, S_{prod}, relative to that of [1-^{13}C]pyruvate's integrated signal intensity observed for each species selective excitation, $S_{pyr\_product}$, taking into account the respective response coefficient.

The LDH and ALT activities ratio was determined using Equation (2), as the ratio of the production rate of [1-^{13}C]lactate and [1-^{13}C]alanine. As the repetition time, the concentration of extracellular hyperpolarized [1-^{13}C]pyruvate, and the tissue weight were the same for both products; their effects cancel out when calculating the activities ratio. For this reason, the activities ratio is technically a robust parameter.

$$\frac{\nu_{lac}}{\nu_{ala}} = \frac{S_{lac} \cdot \rho_{lac}}{S_{pyr\_lac}} \cdot \frac{S_{pyr\_ala}}{S_{ala} \cdot \rho_{ala}} \quad (2)$$

For each injection, only data points with high signal-to-noise ratio of both [1-^{13}C]lactate and the [1-^{13}C]alanine signals were selected for this analysis. Additionally, the first point was omitted, due to the fact that the time for which [1-^{13}C]lactate and [1-^{13}C]alanine production occurred could not be determined.

5.8. Parameters Used for Enzymatic Rate Calculations

The parameters used for enzymatic rate calculations per animal per injection of hyperpolarized [1-^{13}C]pyruvate are summarized in Table 1. The entire data set described in Table 1 was used to reach the results described in Figure 3 in the text. The product-selective RF pulse profiles and the determination of the relative responses of the product and the substrate (ρ in Table 1) were previously described by Adler-Levi et al. [40] (2.5 ms Sinc pulse) and Lev-Cohain et al. [21] (3 ms Gaussian pulse). The enzymatic rates obtained from healthy animals (Mice number 1–3 in Table 1) were published previously in Lev-Cohain et al. [21]. Here, these enzymatic rates were re-calculated using only a few time points from each experiment, applying more rigorous selection criteria based on SNR to match the quality of the diseased animal data which had better SNR.

Author Contributions: N.L.-C., conceptualization, data curation, investigation, writing–original draft, writing—review and editing; G.S., conceptualization, data curation, formal analysis, investigation, writing–original draft, writing—review and editing; S.U., data curation, formal analysis, investigation, writing—review and editing; A.N.-S., methodology, writing—review and editing; S.N.G., conceptualization, methodology, resources, writing—review and editing; Y.A.-L., writing—review and editing; J.S., conceptualization, resources, writing—review and editing; J.M.G., conceptualization, resources, writing—review and editing; R.K.-B., conceptualization, funding acquisition, investigation, methodology, project administration, resources, supervision, validation, writing—original draft, writing—review and editing. All authors have read and agreed to the published version of the manuscript.

Funding: This project has received partial funding from the European Research Council (ERC) under grant agreement No. 338040, the European Union's Horizon 2020 research and innovation program under grant agreement No. 667192, and the Israeli Ministry of Science and Technology. A.N.-S. received the Golda Meir Award under grant agreement number 0395111.

Data Availability Statement: The data presented in this study are available on request from the corresponding author.

Acknowledgments: We thank Ayelet Gamliel for the preparation of formulations for polarization and dissolution buffers, Assad Azar for technical support with slice preparation and perfusion, and Talia Harris for assistance with calibrations of the NMR spectrometer and selective pulses. We thank Eli Pikarsky for the histological analysis of the PCLS used in the metabolic studies.

Conflicts of Interest: There are no conflicts of interests. Goldberg SN is a consultant to Angiodynamics, Cosman Company, and Xact Robotics.

Abbreviations

dDNP	dissolution dynamic nuclear polarization
LDH	lactate dehydrogenase
ALT	alanine transaminase
TR	repetition time

References

1. Forner, A.; Bruix, J. Biomarkers for early diagnosis of hepatocellular carcinoma. *Lancet Oncol.* **2012**, *13*, 750–751. [CrossRef]
2. Llovet, J.M.; Bru, C.; Bruix, J. Prognosis of hepatocellular carcinoma: The BCLC staging classification. *Semin. Liver Dis.* **1999**, *19*, 329–338. [CrossRef] [PubMed]
3. Ardenkjær-Larsen, J.H.; Fridlund, B.; Gram, A.; Hansson, G.; Hansson, L.; Lerche, M.H.; Servin, R.; Thaning, M.; Golman, K. Increase in signal-to-noise ratio of >10,000 times in liquid-state NMR. *Proc. Natl. Acad. Sci. USA* **2003**, *100*, 10158–10163. [CrossRef] [PubMed]
4. Duwel, S.; Durst, M.; Gringeri, C.V.; Kosanke, Y.; Gross, C.; Janich, M.A.; Haase, A.; Glaser, S.J.; Schwaiger, M.; Schulte, R.F.; et al. Multiparametric human hepatocellular carcinoma characterization and therapy response evaluation by hyperpolarized C-13 MRSI. *NMR Biomed.* **2016**, *29*, 952–960. [CrossRef]
5. Darpolor, M.M.; Kaplan, D.E.; Pedersen, P.L.; Glickson, J.D. Human hepatocellular carcinoma metabolism: Imaging by hyperpolarized ^{13}C magnetic resonance spectroscopy. *J. Liver Dis. Transpl.* **2012**, *1*, 1. [CrossRef]
6. Cunningham, C.H.; Lau, J.Y.C.; Chen, A.P.; Geraghty, B.J.; Perks, W.J.; Roifman, I.; Wright, G.A.; Connelly, K.A. Hyperpolarized ^{13}C metabolic MRI of the human heart initial experience. *Circ. Res.* **2016**, *119*, 1177–1182. [CrossRef]
7. Nelson, S.J.; Kurhanewicz, J.; Vigneron, D.B.; Larson, P.E.Z.; Harzstark, A.L.; Ferrone, M.; Criekinge, M.; Chang, J.W.; Bok, R.; Park, I.; et al. Metabolic imaging of patients with prostate cancer using hyperpolarized [1-^{13}C] pyruvate. *Sci. Transl. Med.* **2013**, *5*, 198ra108. [CrossRef]
8. Park, I.; Autry, A.; Yang, X.D.; Zhai, Y.Y.; Sriram, R.; Korenchan, D.; Kurhanewicz, J.; Cunha, A.; Hsu, I.C.; Nelson, S.; et al. Noninvasive assessment of treatment response for diffuse intrinsic pontine glioma using hyperpolarized ^{13}C metabolic imaging. *Neurooncol. Pract.* **2017**, *19*, 194.
9. Chung, B.T.; Chen, H.Y.; Gordon, J.; Mammoli, D.; Sriram, R.; Autry, A.W.; Page, L.M.; Chaumeil, M.M.; Shin, P.; Slater, J.; et al. First hyperpolarized 2-^{13}C pyruvate MR studies of human brain metabolism. *J. Magn. Reson.* **2019**, *309*, 106617. [CrossRef]
10. Kurhanewicz, J.; Vigneron, D.B.; Ardenkjaer, L.J.H.; Bankson, J.A.; Brindle, K.; Cunningham, C.H.; Gallagher, F.A.; Keshari, K.R.; Kjaer, A.; Laustsen, C.; et al. Hyperpolarized ^{13}C MRI: Path to Clinical Translation in Oncology. *Neoplasia* **2019**, *21*, 1–16. [CrossRef]
11. Fussenich, L.M.; Desar, I.M.E.; Peters, M.; Teerenstra, S.; Graaf, W.T.A.; Timmer-Bonte, J.N.H.; Herpen, C.M.L. A new, simple and objective prognostic score for phase I cancer patients. *Eur. J. Cancer* **2011**, *47*, 1152–1160. [CrossRef] [PubMed]
12. Girgis, H.; Masui, O.; White, N.M.A.; Scorilas, A.; Rotondo, F.; Seivwright, A.; Gabril, M.; Filter, E.R.; Girgis, A.H.A.; Bjarnason, G.A.; et al. Lactate dehydrogenase A is a potential prognostic marker in clear cell renal cell carcinoma. *Mol. Cancer* **2014**, *13*, 101. [CrossRef] [PubMed]
13. Lee, T.H.; Kim, W.R.; Benson, J.T.; Therneau, T.M.; Melton, L.J. Serum aminotransferase activity and mortality risk in a United States community. *Hepatology* **2008**, *47*, 880–887. [CrossRef]
14. Sherman, K.E. Alanine aminotransferase in clinical-practice—A review. *Arch. Intern. Med.* **1991**, *151*, 260–265. [CrossRef] [PubMed]
15. Yang, R.Z.; Park, S.; Reagan, W.J.; Goldstein, R.; Zhong, S.; Lawton, M.; Rajamohan, F.; Qian, K.; Liu, L.; Gong, D.W.; et al. Alanine aminotransferase isoenzymes: Molecular cloning and quantitative analysis of tissue expression in rats and serum elevation in liver toxicity. *Hepatology* **2009**, *49*, 598–607. [CrossRef]

16. Bilgic, I.; Gelecek, S.; Akgun, A.E.; Ozmen, M.M. Predictive value of liver transaminases levels in abdominal trauma. *Am. J. Emerg. Med.* **2014**, *32*, 705–708. [CrossRef]
17. Park, J.M.; Khemtong, C.; Liu, S.C.; Hurd, R.E.; Spielman, D.M. In vivo assessment of intracellular redox state in rat liver using hyperpolarized 1-^{13}C Alanine. *Magn. Reson. Med.* **2017**, *77*, 1741–1748. [CrossRef]
18. Hu, S.; Chen, A.P.; Zierhut, M.L.; Bok, R.; Yen, Y.F.; Schroeder, M.A.; Hurd, R.E.; Nelson, S.J.; Kurhanewicz, J.; Vigneron, D.B. In vivo carbon-13 dynamic MRS and MRSI of normal and fasted rat liver with hyperpolarized ^{13}C-pyruvate. *Mol. Imaging Biol.* **2009**, *11*, 399–407. [CrossRef]
19. Jin, E.S.; Moreno, K.X.; Wang, J.X.; Fidelino, L.; Merritt, M.E.; Sherry, A.D.; Malloy, C.R. Metabolism of hyperpolarized [1-^{13}C] pyruvate through alternate pathways in rat liver. *NMR Biomed.* **2016**, *29*, 466–474. [CrossRef]
20. Lee, P.; Leong, W.; Tan, T.; Lim, M.; Han, W.P.; Radda, G.K. In vivo hyperpolarized carbon-13 magnetic resonance spectroscopy reveals increased pyruvate carboxylase flux in an insulin-resistant mouse model. *Hepatology* **2013**, *57*, 515–524. [CrossRef]
21. Lev-Cohain, N.; Sapir, G.; Harris, T.; Azar, A.; Gamliel, A.; Nardi-Schreiber, A.; Uppala, S.; Sosna, J.; Gomori, J.M.; Katz-Brull, R. Real-time ALT and LDH activities determined in viable precision-cut mouse liver slices using hyperpolarized 1-^{13}C pyruvate-Implications for studies on biopsied liver tissues. *NMR Biomed.* **2019**, *32*, e4043. [CrossRef] [PubMed]
22. Merritt, M.E.; Harrison, C.; Sherry, A.D.; Malloy, C.R.; Burgess, S.C. Flux through hepatic pyruvate carboxylase and phosphoenolpyruvate carboxykinase detected by hyperpolarized ^{13}C magnetic resonance. *Proc. Natl. Acad. Sci. USA* **2011**, *108*, 19084–19089. [CrossRef] [PubMed]
23. Moreno, K.X.; Moore, C.L.; Burgess, S.C.; Sherry, A.D.; Malloy, C.R.; Merritt, M.E. Production of hyperpolarized (CO_2)-^{13}C from 1-^{13}C pyruvate in perfused liver does reflect total anaplerosis but is not a reliable biomarker of glucose production. *Metabolomics* **2015**, *11*, 1144–1156. [CrossRef] [PubMed]
24. Spielman, D.M.; Mayer, D.; Yen, Y.F.; Tropp, J.; Hurd, R.E.; Pfefferbaum, A. In vivo measurement of ethanol metabolism in the rat liver using magnetic resonance spectroscopy of hyperpolarized 1-^{13}C pyruvate. *Magn. Reson. Med.* **2009**, *62*, 307–313. [CrossRef] [PubMed]
25. Golman, K.; Zandt, R.; Thaning, M. Real-time metabolic imaging. *Proc. Natl. Acad. Sci. USA* **2006**, *103*, 11270–11275. [CrossRef] [PubMed]
26. Lewis, A.J.M.; Miller, J.; McCallum, C.; Rider, O.; Neubauer, S.; Heather, L.; Tyler, D.J. Non-invasive assessment of metformin induced changes in cardiac and hepatic redox state using hyperpolarized 1-^{13}C pyruvate. *Heart* **2016**, *102*, A14. [CrossRef]
27. Josan, S.; Billingsley, K.; Orduna, J.; Park, J.M.; Luong, R.; Yu, L.Q.; Hurd, R.; Pfefferbaum, A.; Spielman, D.; Mayer, D.; et al. Assessing inflammatory liver injury in an acute CCl4 model using dynamic 3D metabolic imaging of hyperpolarized 1-^{13}C pyruvate. *NMR Biomed.* **2015**, *28*, 1671–1677. [CrossRef]
28. Katzenellenbogen, M.; Pappo, O.; Barash, H.; Klopstock, N.; Mizrahi, L.; Olam, D.; Jacob-Hirsch, J.; Amariglio, N.; Rechavi, G.; Mitchell, L.A.; et al. Multiple adaptive mechanisms to chronic liver disease revealed at early stages of liver carcinogenesis in the Mdr2-knockout mice. *Cancer Res.* **2006**, *66*, 4001–4010. [CrossRef]
29. Mauad, T.H.; Nieuwkerk, C.M.; Dingemans, K.P.; Smit, J.J.; Schinkel, A.H.; Notenboom, R.G.; Bergh, W.M.A.; Verkruisen, R.P.; Groen, A.K.; Oude, E.R.P. Mice with homozygous disruption of the mdr2 P-glycoprotein gene. A novel animal model for studies of nonsuppurative inflammatory cholangitis and hepatocarcinogenesis. *Am. J. Pathol.* **1994**, *145*, 1237–1245.
30. Katzenellenbogen, M.; Mizrahi, L.; Pappo, O.; Klopstock, N.; Olam, D.; Barash, H.; Domany, E.; Galun, E.; Goldenberg, D. Molecular mechanisms of the chemopreventive effect on hepatocellular carcinoma development in Mdr2 knockout mice. *Mol. Cancer. Ther.* **2007**, *6*, 1283–1291. [CrossRef]
31. Bovenkamp, M.; Groothuis, G.M.M.; Meijer, D.K.F.; Olinga, P. Liver slices as a model to study fibrogenesis and test the effects of anti-fibrotic drugs on fibrogenic cells in human liver. *Toxicol. In Vitro* **2008**, *22*, 771–778. [CrossRef] [PubMed]
32. Bovenkamp, M.; Groothuis, G.M.M.; Meijer, D.K.F.; Olinga, P. Liver fibrosis in vitro: Cell culture models and precision-cut liver slices. *Toxicol. In Vitro* **2007**, *21*, 545–557. [CrossRef] [PubMed]
33. Harris, T.; Uppala, S.; Lev-Cohain, N.; Adler-Levy, Y.; Shaul, D.; Nardi-Schreiber, A.; Sapir, G.; Azar, A.; Gamliel, A.; Sosna, J.; et al. Hyperpolarized product selective saturating-excitations for determination of changes in metabolic reaction rates in real-time. *NMR Biomed.* **2020**, *33*, e4189. [CrossRef] [PubMed]
34. Zhang, J.P.; Wang, H.B.; Lin, Y.H.; Xu, J.; Wang, J.; Wang, K.; Liu, W.L. Lactate dehydrogenase is an important prognostic indicator for hepatocellular carcinoma after partial hepatectomy. *Transl. Oncol.* **2015**, *8*, 497–503. [CrossRef] [PubMed]
35. Moon, C.-M.; Shin, S.-S.; Heo, S.-H.; Lim, H.-S.; Moon, M.-J.; Surendran, S.P.; Kim, G.-E.; Park, I.-W.; Jeong, Y.-Y. Metabolic changes in different stages of liver fibrosis: In vivo hyperpolarized ^{13}C MR spectroscopy and metabolic imaging. *Mol. Imaging Biol.* **2019**, *21*, 842–851. [CrossRef]
36. Chibaudel, B.; Bonnetain, F.; Tournigand, C.; Bengrine-Lefevre, L.; Teixeira, L.; Artru, P.; Desramé, J.; Larsen, A.K.; André, T.; Louvet, C.; et al. Simplified prognostic model in patients with oxaliplatin-based or irinotecan-based first-line chemotherapy for metastatic colorectal cancer: A GERCOR study. *Oncologist* **2011**, *16*, 1228–1238. [CrossRef]
37. Motzer, R.J.; Mazumdar, M.; Bacik, J.; Berg, W.; Amsterdam, A.; Ferrara, J. Survival and prognostic stratification of 670 patients with advanced renal cell carcinoma. *J. Clin. Oncol.* **1999**, *17*, 2530–2540. [CrossRef]
38. Faloppi, L.; Scartozzi, M.; Bianconi, M.; Baroni, G.S.; Toniutto, P.; Giampieri, R.; Prete, M.; Minicis, S.; Bitetto, D.; Loretelli, C.; et al. The role of LDH serum levels in predicting global outcome in HCC patients treated with sorafenib: Implications for clinical management. *BMC Cancer* **2014**, *14*. [CrossRef]

39. Kim, W.R.; Flamm, S.L.; Di Bisceglie, A.M.; Bodenheimer, H.C. Public policy committee of the american association for the study of liver disease. Serum activity of alanine aminotransferase (ALT) as an indicator of health and disease. *Hepatology* **2008**, *47*, 1363–1370. [CrossRef]
40. Adler-Levy, Y.; Nardi-Schreiber, A.; Harris, T.; Shaul, D.; Uppala, S.; Sapir, G.; Lev-Cohain, N.; Sosna, J.; Goldberg, S.N.; Gomori, J.M.; et al. In-cell determination of lactate dehydrogenase activity in a luminal breast cancer model—*Ex vivo* investigation of excised xenograft tumor slices using dDNP hyperpolarized [1-^{13}C]pyruvate. *Sensors* **2019**, *19*, 2089. [CrossRef]